J|A|C|S ARTICLES

Structures of β-Amyloid Peptide 1−40, 1−42, and 1−55—the 672−726 Fragment of APP—in a Membrane Environment with Implications for Interactions with γ-Secretase

Naoyuki Miyashita,[†,‡] John E. Straub,[*,†,§] and D. Thirumalai[∥]

Department of Chemistry, Boston University, Boston, Massachusetts 02215, Department of Chemistry and Biochemistry, Montana State University, Bozeman, Montana 59717, and Biophysics Program, IPST, University of Maryland, College Park, Maryland 20742

Received July 2, 2009; E-mail: straub@bu.edu

Abstract: Aggregation of Amyloid β (Aβ) peptide has been linked to the neurodegenerative Alzheimer's Disease and implicated in other amyloid diseases including cerebral amyloid angiopathy. Aβ peptide is generated by cleavage of the amyloid precursor protein (APP) by transmembrane proteases. It is crucial to determine the structures of β-amyloid peptides in a membrane to provide a molecular basis for the cleavage mechanism. We report the structures of amyloid β peptide (A$β_{1-40}$ and A$β_{1-42}$) as well as the 672−726 fragment of APP (referred to as A$β_{1-55}$) in a membrane environment determined by replica-exchange molecular dynamics simulation. A$β_{1-40}$ is found to have two helical domains A (13−22) and B(30−35) and a type I β-turn at 23−27. The peptide is localized at the interface between membrane and solvent. Substantial fluctuations in domain A are observed. The dominant simulated tertiary structure of A$β_{1-40}$ is observed to be similar to the simulated A$β_{1-42}$ structure. However, there are differences observed in the overall conformational ensemble, as characterized by the two-dimensional free energy surfaces. The fragment of APP (A$β_{1-55}$) is observed to have a long transmembrane helix. The position of the transmembrane region and ensemble of membrane structures are elucidated. The conformational transition between the transmembrane A$β_{1-55}$ structure, prior to cleavage, and the A$β_{1-40}$ structure, following cleavage, is proposed.

Introduction

It has been proposed that the aggregation/oligomerization of Aβ peptides is an essential element of the pathogenicity of Alzheimer's Disease (AD).[1−5] The Aβ peptide is a product of cleavage of the Amyloid Precursor Protein (APP)[6] by two steps. APP, a type I transmembrane (TM) protein composed of 695−770 amino acid residues, is cleaved by β-secretase (BASE) at the β-site between residues 671 and 672. The resulting cleavage product is referred to as APP-C99. Cleavage of APP-C99 by γ-secretase occurs at the γ-site near residues 709−715.[7] To provide a molecular basis for Aβ-aggregation, it is crucial to understand the structures of APP and the Aβ peptide in a membrane, which have eluded experimental determination.

Several isoforms of Aβ peptide have been isolated in vivo including A$β_{1-38}$, A$β_{1-39}$, A$β_{1-40}$, A$β_{1-42}$, and A$β_{1-43}$. A$β_{1-40}$ is the predominant sequence isolated from cerebrospinal fluid,[8,9] while A$β_{1-42}$ is the predominant component of senile plaques in parenchyma.[10,11]

Evidence suggests that Aβ peptides can form not only fibril structures[12−17] and soluble oligomers[18−21] in solution but also cation-selective channels spanning lipid bilayers.[22−25] The low resolution structure of Aβ peptide channels arranged on a membrane surface has been probed using atomic force micros-

[†] Boston University.
[‡] Current address: RIKEN Computational Science Research Program, 2-1 Hirosawa, Wako, Saitama 351-0198, Japan.
[§] Montana State University.
[∥] University of Maryland.

(1) Iversen, L.; Mortishire-Smith, R.; Pollack, S.; Shearman, M *Biochem. J.* **1995**, *311*, 1–16.
(2) Pike, C.; Walencewicz-Wasserman, A.; Kosmoski, J.; Cribbs, D.; Glabe, C.; Cotman, C. *J. Neurochem.* **1995**, *64*, 253–265.
(3) Simmons, L.; May, P.; Tomaselli, K.; Rydel, R.; Fuson, K.; Brigham, E.; Wright, S.; Lieberburg, I.; Becker, G.; Brems, D. *Mol. Pharm.* **1994**, *45*, 373–379.
(4) Lynn, D. G.; Meredith, S. C. *J. Struct. Biol.* **2000**, *130*, 153–173.
(5) Haass, C.; Selkoe, D. J. *Nat. Rev. Mol. Cell. Biol.* **2007**, *8*, 101–112.
(6) Kang, J.; Lemaire, H.; Unterbeck, A.; Salbaum, J.; Masters, C.; Grzeschik, K.; Multhaup, G.; Beyreuther, K.; Müller-Hill, B. *Nature* **1987**, *325*, 733–736.
(7) Vassar, R.; Citron, M. *Neuron* **2000**, *27*, 419–422.

(8) Haass, C.; Schlossmacher, M.; Hung, A.; Vigo-Pelfrey, C.; Mellon, A.; Ostaszewski, B.; Lieberburg, I.; Koo, E.; Schenk, D.; Teplow, D. *Nature* **1992**, *359*, 322–325.
(9) Seubert, P.; Vigo-Pelfrey, C.; Esch, F.; Lee, M.; Dovey, H.; Davis, D.; Sinha, S.; Schlossmacher, M.; Whaley, J.; Swindlehurst, C. *Nature* **1992**, *359*, 325–357.
(10) Masters, C.; Simms, G.; Weinman, N.; Multhaup, G.; McDonald, B.; Beyreuther, K. *Proc. Natl. Acad. Sci. U. S. A.* **1985**, *82*, 4245–4249.
(11) Iwatsubo, T.; Odaka, A.; Suzuki, N.; Mizusawa, H.; Nukina, N.; Ihara, Y. *Neuron* **1994**, *13*, 45–53.
(12) Serpell, L. *Biochim. Biophys. Acta* **2000**, *1502*, 16–30.
(13) Petkova, A.; Ishii, Y.; Balbach, J.; Antzutkin, O.; Leapman, R.; Delaglio, F.; Tycko, R. *Proc. Natl. Acad. Sci. U. S. A.* **2002**, *99*, 16742–16747.
(14) Tycko, R. *Curr. Opin. Struct. Biol.* **2004**, *14*, 96–103.
(15) Lührs, T.; Ritter, C.; Adrian, M.; Riek-Loher, D.; Bohrmann, B.; Döbeli, H.; Schubert, D.; Riek, R. *Proc. Natl. Acad. Sci. U. S. A.* **2005**, *102*, 17342–17347.
(16) Sato, T.; Kienlen-Campard, P.; Ahmed, M.; Liu, W.; Li, H.; Elliott, J.; Aimoto, S.; Constantinescu, S.; Octave, J.; Smith, S. O. *Biochemistry* **2006**, *45*, 5503–5516.
(17) Petkova, A.; Yau, W.; Tycko, R. *Biochemistry* **2006**, *45*, 498–512.

copy (AFM) imaging.[26] Aβ_{1-40} peptide consists of the fragments of APP including 28 residues lying outside the membrane and the first 12 amino acids of the TM portion (Gly$_{700}$-Leu$_{723}$) of APP. It is reasonable to conjecture that monomeric Aβ peptide may be located in the membrane after it is produced from cleavage of APP. The critical evaluation of that conjecture is a principal focus of this study.

The structure of the peptide residues 23−27, which contain the VGSN motif, is of great interest given its importance as an essential turn region in solid-state NMR fibril structures as well as solution phase NMR structures in both aqueous[27] and membrane-mimicking[28−32] solutions. First identified by Kirschner[33] as a probable turn region essential to the Aβ fibril cross-β structure, the VGSN turn has subsequently been confirmed to be an essential component of aggregation-competent Aβ peptide structures.[13,15,17,34−41]

Structures of the Aβ_{1-40} and Aβ_{1-42} peptide monomers in a membrane-mimicking (lower dielectric constant) solvent environment, such as SDS micelle/water complex, TFE/water complex, and HFIP/water complex, have been determined by NMR spectroscopy.[28−32] In each of these structures, the Aβ peptide consists of two helical domains (domain A and B) separated by a kink or turn region. NMR studies of the Aβ peptide in an SDS micelle/water complex environment[30] and complementary molecular dynamics (MD) simulation studies[42] have suggested that it may reside predominantly on the micelle/membrane surface rather than being imbedded in the hydrophobic interior.[30]

Simulations of short and important Aβ fragments (including Aβ_{16-22}, Aβ_{21-30}, Aβ_{10-35}, Aβ_{1-40}, Aβ_{1-42}) in aqueous solution,[34−41,43−52] in aqueous urea solution,[53] and in HFIP/water solution[54] have been investigated. Several studies of the Aβ peptide in a membrane environment using molecular dynamics simulation have been reported.[42,55−57] In a pioneering study, the insertion of the Aβ_{1-40} and Aβ_{1-42} peptides into an implicit membrane model was studied using Monte Carlo simulation.[58] Differences in the degree of insertion of the two peptides were noted and attributed to differences in peptide sequence. The activity of enzymes that function in a membrane environment can be influenced by membrane composition and structure. Marenchino et al. reported that the activity of α-secretase is influenced by details of the membrane environment.[59] It is reasonable to assume that consideration of APP and APP-C99 protein structure and fluctuations in the membrane region will be important to a complete understanding of the relative level of production of Aβ peptide isoforms.

In order to characterize the ensemble of Aβ_{1-40} peptide structures in the membrane environment, we have investigated the structure of monomeric Aβ_{1-40} peptide (DAEFR HDSGY EVHHQ KLVFF AEDVG SNKGA IIGLM VGGVV) in an implicit membrane environment using replica-exchange molecular dynamics (REMD) simulation.[60] The structures are described in terms of the interdomain angle between domain A and B, the tilt angle of domain B, and the depth of insertion of the peptide into the membrane. The ensemble of structures are clustered and projected on to a free energy surface that defines the relative stability and interconnectedness of the dominant structural basins.

(18) Lambert, M.; Barlow, A.; Chromy, B.; Edwards, C.; Freed, R.; Liosatos, M.; Morgan, T.; Rozovsky, I.; Trommer, B.; Viola, K.; Wals, P.; Zhang, C.; Finch, C.; Krafft, G.; Klein, W. *Proc. Natl. Acad. Sci. U. S. A.* **1998**, *95*, 6448–6453.

(19) Walsh, D.; Hartley, D.; Kusumoto, Y.; Fezoui, Y.; Condron, M.; Lomakin, A.; Benedek, G.; Selkoe, D.; Teplow, D. *J. Biol. Chem.* **1999**, *274*, 25945–25952.

(20) Hardy, J.; Selkoe, D. *Science* **2002**, *297*, 353–356.

(21) Mastrangelo, I. A.; Ahmed, M.; Sato, T.; Liu, W.; Wang, C.; Hough, P.; Smith, S. O. *J. Mol. Biol.* **2006**, *358*, 106–119.

(22) Arispe, N.; Rojas, E.; Pollard, H. *Proc. Natl. Acad. Sci. U. S. A.* **1993**, *90*, 567–571.

(23) Arispe, N.; Pollard, H.; Rojas, E. *Proc. Natl. Acad. Sci. U. S. A.* **1993**, *90*, 10573–10577.

(24) Kawahara, M.; Arispe, N.; Kuroda, Y.; Rojas, E. *Biophys. J.* **1997**, *73*, 67–75.

(25) Jang, H.; Ma, B.; Lal, R.; Nussinov, R. *Biophys. J.* **2008**, *95*, 4631–4642.

(26) Lin, H.; Bhatia, R.; Lal, R. *FASEB J.* **2001**, *15*, 2433–2444.

(27) Zheng, J.; Jang, H.; Ma, B.; Nussinov, R. *J. Phys. Chem. B* **2008**, *112*, 6856–6865.

(28) Sticht, H.; Bayer, P.; Willbold, D.; Dames, S.; Hilbich, C.; Beyreuther, K.; Frank, R.; Rösch, P. *Eur. J. Biochem.* **1995**, *233*, 293–298.

(29) Coles, M.; Bicknell, W.; Watson, A.; Fairlie, D.; Craik, D. *Biochemistry* **1998**, *37*, 11064–11077.

(30) Shao, H.; Jao, S.; Ma, K.; Zagorski, M. *J. Mol. Biol.* **1999**, *285*, 755–773.

(31) Crescenzi, O.; Tomaselli, S.; Guerrini, R.; Salvadori, S.; D'Ursi, A.; Temussi, P.; Picone, D. *Eur. J. Biochem.* **2002**, *269*, 5642–5648.

(32) Tomaselli, S.; Esposito, V.; Vangone, P.; van Nuland, N. A. J.; Bonvin, A. M. J. J.; Guerrini, R.; Tancredi, T.; Temussi, P. A.; Picone, D. *Chembiochem* **2006**, *7*, 257–267.

(33) Kirschner, D. A.; Inouye, H.; Duffy, L. K.; Sinclair, A.; Lind, M.; Selkoe, D. J. *Proc. Natl. Acad. Sci. U. S. A.* **1987**, *84*, 6953–6957.

(34) Massi, F.; Peng, J. W.; Lee, J. P.; Straub, J. E. *Biophys. J.* **2001**, *80*, 31–44.

(35) Massi, F.; Straub, J. E. *Proteins* **2001**, *42*, 217–229.

(36) Massi, F.; Straub, J. E. *Biophys. J.* **2001**, *81*, 697–709.

(37) Tarus, B.; Straub, J.; Thirumalai, D. *J. Am. Chem. Soc.* **2006**, *128*, 16159–16168.

(38) Tarus, B.; Straub, J. E.; Thirumalai, D. *J. Mol. Biol.* **2008**, *379*, 815–829.

(39) Borreguero, J. M.; Urbanc, B.; Lazo, N. D.; Buldyrev, S. V.; Teplow, D. B.; Stanley, H. E. *Proc. Natl. Acad. Sci. U. S. A.* **2005**, *102*, 6015–6020.

(40) Cruz, L.; Urbanc, B.; Borreguero, J. M.; Lazo, N. D.; Teplow, D. B.; Stanley, H. E. *Proc. Natl. Acad. Sci. U. S. A.* **2005**, *102*, 18258–18263.

(41) Baumketner, A.; Bernstein, S. L.; Wyttenbach, T.; Lazo, N. D.; Teplow, D. B.; Bowers, M. T.; Shea, J.-E. *Protein Sci.* **2006**, *15*, 1239–1247.

(42) Xu, Y.; Shen, J.; Luo, X.; Zhu, W.; Chen, K.; Ma, J.; Jiang, H. *Proc. Natl. Acad. Sci. U. S. A.* **2005**, *102*, 5403–5407.

(43) Jang, S.; Shin, S. *J. Phys. Chem. B* **2006**, *110*, 1955–1958.

(44) Wei, G.; Mousseau, N.; Derreumaux, P. *Prion* **2007**, *1*, 3–8.

(45) Sgourakis, N. G.; Yan, Y.; McCallum, S. A.; Wang, C.; Garcia, A. E. *J. Mol. Biol.* **2007**, *368*, 1448–1457.

(46) Itoh, S. G.; Okamoto, Y. *J. Phys. Chem. B* **2008**, *112*, 2767–2770.

(47) Krone, M. G.; Baumketner, A.; Bernstein, S. L.; Wyttenbach, T.; Lazo, N. D.; Teplow, D. B.; Bowers, M. T.; Shea, J.-E. *J. Mol. Biol.* **2008**, *381*, 221–228.

(48) Murray, M. M.; Krone, M. G.; Bernstein, S. L.; Baumketner, A.; Condron, M. M.; Lazo, N. D.; Teplow, D. B.; Wyttenbach, T.; Shea, J.-E.; Bowers, M. T. *J. Phys. Chem. B* **2009**, *113*, 6041–6046.

(49) Krone, M. G.; Hua, L.; Soto, P.; Zhou, R.; Berne, B. J.; Shea, J.-E. *J. Am. Chem. Soc.* **2008**, *130*, 11066–11072.

(50) Chebaro, Y.; Dong, X.; Laghaei, R.; Derreumaux, P.; Mousseau, N. *J. Phys. Chem. B* **2009**, *113*, 267–274.

(51) Mukherjee, S.; Chowdhury, P.; Gai, F. *J. Phys. Chem. B* **2009**, *113*, 531–535.

(52) Wu, C.; Murray, M. M.; Bernstein, S. L.; Condron, M. M.; Bitan, G.; Shea, J.-E.; Bowers, M. T. *J. Mol. Biol.* **2009**, *387*, 492–501.

(53) Klimov, D.; Straub, J. E.; Thirumalai, D. *Proc. Natl. Acad. Sci. U. S. A.* **2004**, *101*, 14760–14765.

(54) Wei, G.; Shea, J.-E. *Biophys. J.* **2006**, *91*, 1638–1647.

(55) Davis, C. H.; Berkowitz, M. L. *Biophys. J.* **2009**, *96*, 785–797.

(56) Lemkul, J. A.; Bevan, D. R. *Arch. Biochem. Biophys.* **2008**, *470*, 54–63.

(57) Lemkul, J. A.; Bevan, D. R. *FEBS J.* **2009**, *276*, 3060–3075.

(58) Mobley, D. L.; Cox, D. L.; Singh, R. R. P.; Maddox, M. W.; Longo, M. L. *Biophys. J.* **2004**, *86*, 3585–3597.

(59) Marenchino, M.; Williamson, P. T. F.; Murri, S.; Zandomeneghi, G.; Wunderli-Allenspach, H.; Meier, B. H.; Krämer, S. D. *Biophys. J.* **2008**, *95*, 1460–1473.

(60) Sugita, Y.; Okamoto, Y. *Chem. Phys. Lett.* **1999**, *314*, 141–151.

APP is cleaved by β-secretase at the β-site, resulting in the creation of APP-C99. The tertiary structures of the APP and APP-C99 have not been experimentally determined. Currently, the position of the TM domain of APP and APP-C99 is not known exactly.[29,61] To address this question, we have used REMD to simulate the structure of the APP fragment 672−726, referred to as $A\beta_{1-55}$ ($A\beta_{1-40}$ + IATVI VITLV MLKKK), in a membrane environment. We have identified $A\beta_{1-55}$ as a "minimal model" of APP-C99. Differing from APP-C99 only in the truncation of the C-terminal tail region, the $A\beta_{1-55}$ peptide includes all residues of $A\beta_{1-42}$ and all residues identified as being essential to the cleavage of APP-C99 by γ-secretase.[62] The structural ensemble of $A\beta_{1-55}$ interacting with a membrane was characterized in terms of the tilt angle between the z-axis and the TM domain, allowing for the identification of the TM domain region of APP/APP-C99.

Material and Methods

Initial Protein Structures. The initial structure used in the simulation of $A\beta_{1-40}$ was Protein Data Bank (PDB) ID: 1BA4.[29] Two residues, ILE and ALA, were added to the C-terminus of PDB ID: 1BA4 to create the initial structure of $A\beta_{1-42}$, and 15 residues (IATVI VITLV MLKKK) were added to the C-terminus of PDB ID:1BA4 to create the initial structure of $A\beta_{1-55}$.

Implicit Solvation Model of the Membrane. Implicit solvation models are often used to reduce computational time. The appropriateness of an implicit solvation model will depend upon the system studied and the paticular observables of interest. For certain systems, the use of existing implicit solvent models has been shown to lead to erroneous results.[37] The most dramatic successes of the application of implicit solvation models include the simulation of protein insertion in membranes.[63−66] Our calculations were performed using the generalized Born model with a simple switching function (GBSW)[65−68] in the CHARMM program.[69] GBSW is one of the more popular implicit solvent models and captures the essential character of the membrane/water interface. Use of the GBSW solvation model can dramatically reduce the simulation time and lead to substantially enhanced sampling of the protein conformations by removing steric contacts with explicit solvent and lipid molecules. It has been argued that the GBSW method closely approximates the energetics of the Poisson−Boltzmann solvation model. The interfacial region between the solvent and lipid region of the membrane was modeled using a continuous and smooth switching function.

The PARAM22 force field with dihedral cross-term corrections (CMAP)[67] was used. The time-step was 2 fs with a cutoff distance of 20 Å. The smoothing length was 0.6 Å at the dielectric boundary, defined by the optimized Poisson−Boltzmann atomic radii for proteins with 24 radial integration points and up to 20 Å and 38 angular integration points. A surface tension coefficient of 0.04 kcal/mol $Å^2$ was used. The profile of the membrane consists of a 25 Å hydrophobic core with a 5 Å membrane/solvent interface on either side.

Several continuum dielectric membrane models are commonly employed. These models provide approximate "mean field" energetics but lack fluctuations in the shape of the membrane and the disorder characteristic of more detailed atomistic membrane models. Using a coarse-grained model of the membrane provides a dramatically enhanced sampling for the peptide conformational ensemble using REMD. To assess the adequacy of the model employed for the problems studied, we compared our simulation results for the structure of the shorter $A\beta_{1-40}$ and $A\beta_{1-42}$ peptides with (1) the results of a study using an all atom model of peptide, membrane, and solvent[42] and (2) existing experimental results derived from solution NMR studies of the $A\beta_{1-40}$ and $A\beta_{1-42}$ peptides in nonpolar solvent and micelle environments.[28−32] That comparison (see Results) suggests the appropriateness of the approximate membrane model and REMD sampling method used for our study of the structure of the longer $A\beta_{1-55}$ peptide for which there is no experimental structure.

REMD Simulation. Replica-exchange molecular dynamics (REMD) simulation is a popular enhanced conformational sampling method.[60] The dynamics of noninteracting replicas of the system, each at a specified temperature, are calculated by traditional MD simulation. Pairs of replicas that have nearest neighbor temperatures are exchanged every few steps using the Metropolis criterion to ensure detailed balance. Each replica may diffuse through temperature space which helps to avoid being trapped in a local basin of the potential energy surface. As a result, the REMD method can sample a wider conformational space than traditional MD simulation.

We used 32 replicas spanning a temperature range of 300−700 K. The exchange frequency between nearest neighbor replicas was every 2 ps and the exchange ratios averaged between 24−40%. The total simulation length was 10 ns for each replica. The total simulation lengths were 320 ns for $A\beta_{1-40}$ and 320 ns for $A\beta_{1-55}$. The initial 4 ns (128 ns in total) of each simulation was discarded to avoid any dependence on the initial protein structure. To manage the REMD simulations, we used the MMTSB tool set.[70]

Analysis. The weighted histogram analysis method (WHAM)[71] was applied to the analysis of all simulations discussed. The secondary-structure assignments used the DSSP definition[72] based on hydrogen bonding informed by electrostatic energy calculations.

Results

The Structure of $A\beta_{1-40}$ in a Membrane Environment. We simulated $A\beta_{1-40}$ in a membrane environment using REMD. The average secondary-structure of the protein at 300 K was analyzed using DSSP[72] and the weighted histogram analysis method (WHAM).[71] The averaged occupancies of α-helix, 3/10-helix, hydrogen bonded turn, bend, and coil components are shown in Figure 1(a). The two α-helical components characterize the structure of the protein, whereas β-sheet components were rarely observed. These observations are consistent with the general tendency of peptides to assume helical structures in a membrane environment, and with existing NMR structures for $A\beta_{1-40}$ in a TFE/water, HFIP/water, or SDS micelle environment. The sequence 1−12 is a coil, 13−22 a helix (domain A), 23−29 a turn, 30−35 a helix (domain B), and 36−40 a coil. Domain A can be further divided into subdomains A_I (13−18) and domain A_{II} (19−22). The A_I domain consists of a rigid helix while domain A_{II} is less prominent. Overall, the simulated structures of the $A\beta_{1-40}$ peptide consist of two helical domains separated by a turn region in reasonable agreement with experimentally determined $A\beta$ peptide structures

(61) Beel, A. J.; Mobley, C. K.; Kim, H. J.; Tian, F.; Hadziselimovic, A.; Jap, B.; Prestegard, J. H.; Sanders, C. R. *Biochemistry* **2008**, *47*, 9428−9446.

(62) Funamoto, S.; Morishima-Kawashima, M.; Tanimura, Y.; Hirotani, N.; Saido, T.; Ihara, Y. *Biochemistry* **2004**, *43*, 13532−13540.

(63) Roux, B.; Bernèche, S.; Im, W. *Biochemistry* **2000**, *39*, 13295−13306.

(64) Murray, D.; Honig, B. *Mol. Cell* **2002**, *9*, 145−154.

(65) Im, W.; Lee, M.; Brooks III, C. L. *J. Comput. Chem.* **2003**, *24*, 1691−1702.

(66) Im, W.; Feig, M.; Brooks III, C. L. *Biophys. J.* **2003**, *85*, 2900−2918.

(67) Mackerell, F.; Feig, M.; Brooks III, C. L. *J. Comput. Chem.* **2004**, *25*, 1400−1415.

(68) Im, W.; Brooks III, C. L. *J. Mol. Biol.* **2004**, *337*, 513−519.

(69) Brooks, B. R.; Bruccoleri, R. E.; Olafson, B. D.; States, D. J.; Swaminathan, S.; Karplus, M. *J. Comput. Chem.* **1983**, *4*, 187−217.

(70) Feig, M.; Karanicolas, J.; Brooks III, C. L. *MMTSB NIH Research Resource, The Scripps Research Institute* 2001.

(71) Kumar, S.; Rosenberg, J. M.; Bouzida, D.; Swendsen, R. H.; Kollman, P. A. *J. Comput. Chem.* **1992**, *13*, 1011−1021.

(72) Kabsch, W.; Sander, C. *Biopolymers* **1983**, *22*, 2577−2637.
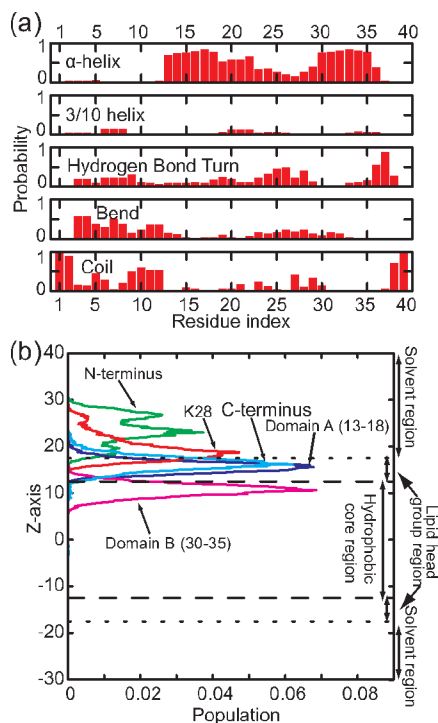
Figure 1. (a) The secondary structure content for residues of Aβ$_{1-40}$ at 300 K. (b) The population of domains and sites of Aβ$_{1-40}$ at 300 K. The dashed and dotted lines indicate the interface between the lipid headgroup region and the hydrophobic core region of the membrane, and the interface between the membrane and solvent, respectively. The positions of the N-terminus (green), domain A (13−18) (blue), N$_\zeta$ of Lys$_{28}$ (red), domain B (30−35) (magenta) and C-terminus (cyan) are shown. The vertical axis indicates the z-axis oriented normal to the membrane surface.

in a variety of membrane-mimicking or lower dielectric solvent environments (see Table 1).[28−32]

Figure 1(b) shows the averaged populations of the central position of the N-terminal residues (green), domain A$_I$ residues 13−18 (blue), N$_\zeta$ of Lys$_{28}$ (red), domain B residues 30−35 (magenta), and C-terminal residues (cyan) as projected onto the z-axis oriented normal to the membrane surface at 300 K. Also indicated are the boundaries between the hydrophobic core region and the lipid headgroup region (dashed line), and the interface between the lipid headgroup region and solvent region (dotted line). In our simulations, the solvent regions have a high dielectric constant (ε = 80), while the hydrophobic core region is assigned a low dielectric constant (ε = 1). The intermediate lipid headgroup region is modeled using a dielectric constant that was scaled linearly between the solvent and membrane interfaces. All components of the Aβ$_{1-40}$ peptide are located on one side of the membrane, while the N-terminal residues are outside of the membrane region. Domain A consists of hydrophobic and hydrophilic residues ^{13}HHQKLV and lies between the hydrophobic core and solvent. N$_\zeta$ of Lys$_{28}$ is located on the interface between the membrane and solvent. Domain B−residues ^{30}AIIGLM−consists of hydrophobic residues, and favors the hydrophobic core regions of the membrane. It is, however, located just below the interface between the lipid headgroup region and the hydrophobic core region, with domain B being elevated by interactions of the C-terminus and Lys$_{28}$ with the solvent.

The principal component analysis (PCA)[73−76] combined with WHAM, which has been used to analyze the total root-mean-square fluctuations of the peptide backbone in studies of the

mechanism of protein folding and stability,[74,77−81] can also be used to classify the structures. We determined the contribution of each principal component (PC). The contributions of the first five PCs to the protein's root-mean square fluctuations are in order: 19.59%, 14.32%, 8.55%, 7.03%, and 5.66%. The first and second PCs contribute 33.91% and may serve as good order parameters. The first and second PC vectors are shown in Figure 2.

The orange horizontal line is the interface between the membrane and solvent, and the green horizontal line indicates the interface between the lipid headgroup region and the hydrophobic core region. The first PC shows domain A sliding in the lipid headgroup region with domain B tilting and inserted into the hydrophobic core region of the membrane. The motion of the first PC is scissor-like [Figure 2 (a)]. In the second PC both domains (A and B) move face-to-face. The motion of the second PC is like that of a nail clipper [Figure 2 (b)].

Figure 3 (a) shows the free energy landscape projected onto the first and second PC axes at 300 K. The free energy was defined as $\Delta G(q_1,q_2) = -k_B T \ln P_B(q_1,q_2)$, where q_1 and q_2 are the first and second PCs, respectively, and $P_B(q_1,q_2)$ is a canonical probability distribution function at temperature T reweighted using WHAM. Three regions and seven local minimum (LM) basins were identified. The first region includes basin Aβ 40PCA-LM1 (PC1, PC2) = (10, 2), LM5 (22, −2) and LM6 (2, 16). The second region includes Aβ 40PCA-LM2 (−10, 2), LM3 (−12, 20), and LM4 (−16, 14). The third region includes Aβ 40PCA-LM7 (−2, 44). The basins were numbered according to the their depth in free energy. The global minimum basin (the basin of lowest free energy) is LM1, while the basin of second lowest free energy is referred to as LM2. The structures of the most populated clusters in each basin are shown in Figure 3(a). The global minimum structure Aβ 40PCA-LM1 has two helical domains that are located on residues 13−22 (domain A) and residues 29−35 (domain B), and the turn region is between residues 23−27.

The free energy landscape at 300K along the inter domain angle (θ), between domain A$_I$ and B, and the tilt angle (α), of the domain B axes, is shown in Figure 3(b). The angles are defined as $\theta = \arccos(\vec{a} \cdot \vec{b}/(|\vec{a}||\vec{b}|))$ and $\alpha = \arccos(\vec{b} \cdot (-\vec{z})/(|\vec{b}||\vec{z}|))$, where $\vec{a}$ is the vector of domain A(13−18), $\vec{b}$ is the vector of domain B (30−35), and $\vec{z}$ is the vector of the z-axis $(0,0,1)^T$. We show seven local minima basins. The global minimum basin (Aβ40θα-LM1) and the second minimum basin (LM2) are located at $(\theta,\alpha) = (63°,45°)$ and $(\theta,\alpha) = (120°,51°)$, respectively.

Figure 3(c) depicts the conformations of each PCA basin whose potential energy is less than −600 kcal/mol projected

(73) Kitao, A.; Hirata, F.; Go, N. *Chem. Phys.* **1991**, *158*, 447–472.
(74) García, A. *Phys. Rev. Lett.* **1992**, *68*, 2696–2699.
(75) Amadei, A.; Linssen, A.; Berendsen, H. *Proteins* **1993**, *17*, 412–425.
(76) Kitao, A.; Go, N. *Curr. Opin. Struct. Biol.* **1999**, *9*, 164–169.
(77) Zhou, R.; Berne, B.; Germain, R. *Proc. Natl. Acad. Sci. U. S. A.* **2001**, *98*, 14931–14936.
(78) Kokubo, H.; Okamoto, Y. *J. Phys. Soc. Jpn.* **2004**, *73*, 2571–2585.
(79) Sugita, Y.; Okamoto, Y *Biophys. J.* **2005**, *88*, 3180–3190.
(80) Gallicchio, E.; Andrec, M.; Felts, A. K.; Levy, R. M. *J. Phys. Chem. B* **2005**, *109*, 6722–6731.
(81) Sugita, Y.; Miyashita, N.; Yoda, T.; Ikeguchi, M.; Toyoshima, C. *Biochemistry* **2006**, *45*, 11752–11761.
(82) Munter, L.-M.; Voigt, P.; Harmeier, A.; Kaden, D.; Gottschalk, K. E.; Weise, C.; Pipkorn, R.; Schaefer, M.; Langosch, D.; Multhaup, G. *EMBO J.* **2007**, *26*, 1702–1712.
(83) Kienlen-Campard, P.; Tasiaux, B.; Hees, J. V.; Li, M.; Huysseune, S.; Sato, T.; Fei, J. Z.; Aimoto, S.; Courtoy, P. J.; Smith, S. O.; Constantinescu, S. N.; Octave, J.-N. *J. Biol. Chem.* **2008**, *283*, 7733–7744.

Table 1. Secondary Structural Regions Determined by Experiment Compared with Our Simulations Results

papers	environment	helices (A and B)	turn, kink	PDB ID
H. Sticht et al.[28]	$A\beta_{1-40}$ in TFE/water	A:15−23, B:31−35	24−30	1AML
M. Coles et al.[29]	$A\beta_{1-40}$ in SDS/water	A:15−24, B:28−36	25−27: Kink	1BA4
H. Shao et al.[30]	$A\beta_{1-42}$ in SDS/water	A:10−24, B:28−42	25−27	
O. Crescenzi et al.[31]	$A\beta_{1-42}$ in the aqueous solution of fluorinated alcohols	A:8−25, B:28−38	26−27: Type I	1IYT
S. Tomaselli et al.[32]	$A\beta_{1-42}$ in HFIP/water	A:10−22, B:28−32	25−26: β-turn	1Z0Q
present work	$A\beta_{1-40}$ in membrane	A:13−22, B:30−35	23−26: Type I β	
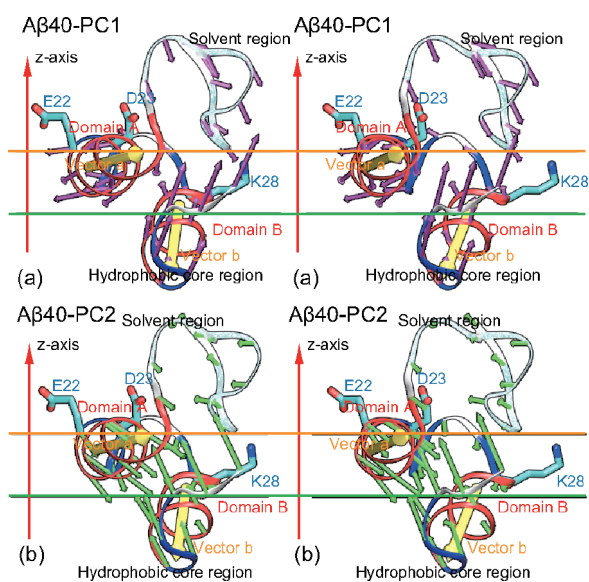
Figure 2. The first (a) and second (b) principal component vectors are shown in stereo (para). The structures are representative of the ensemble of $A\beta_{1-40}$ peptide structures occupying the global minimum of the free energy landscape. The orange and green horizontal lines demonstrate the solvent-membrane and lipid interfaces, respectively. The yellow allows indicate the domain vectors (A$_I$ ($\vec{a}$) and B ($\vec{b}$)). The vectors of the domain (A$_I$ and B) are defined as $\vec{a} = \vec{p}_1 - \vec{p}_2$ and $\vec{b} = \vec{s}_2 - \vec{s}_1$, respectively, where $\vec{p}_1$, $\vec{p}_2$, $\vec{s}_1$, and $\vec{s}_2$ are the averaged position of the center of geometry of the heavy atoms of the residues 12−17, 14−19, 29−34, and 31−36. The purple and green arrows represent the first and second principal component vectors, which indicate fluctuations of the domains. The illustrations were prepared using VMD[85] and Raster3D.[86]

onto the θ and α axes. The major cluster of Aβ 40PCA-LM1 conformations is related to the global minimum basin (Aβ40θα-LM1) on the free energy landscape, though the conformations in basin Aβ40PCA-LM1 can be separated into two groups. The major cluster of Aβ40PCA-LM2 conformations corresponds to Aβ40 θα-LM2 on the θ-α space.

The free energy landscape along the θ and α axes is a flat surface surrounded by high walls. The flatness is due to the significant fluctuation of the inter domain angle θ. The high wall reflects fluctuation of the helix domain motions due to the difference in the dielectric constant between the membrane and solvent. The distribution associated with the global minimum basin (Aβ40PCA-LM1) has a substructure of two minima when expanded along the θ axis (reflecting fluctuations in domain A$_I$). Allowing for fluctuation, the tilt angle of domain B and the inter domain angle would be α ∼ 45° and θ ∼ 63° in the global minimum structure.

The distribution of separations between Asp$_{23}$ O and Ser$_{26}$ HN in Figure 4(a) shows that the most probable separation is 2.2 Å, indicating that the relative positions of Asp$_{23}$ and Ser$_{26}$ are often stabilized by a hydrogen bond. The minimum of the free energy landscape along the φ and ψ axes of Val$_{24}$ and Gly$_{25}$
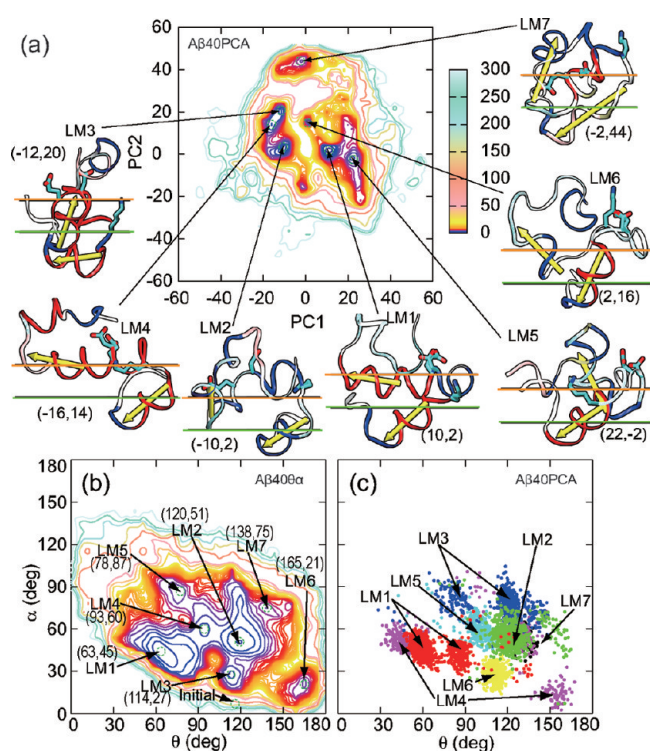
Figure 3. (a) Free energy landscape of $A\beta_{1-40}$ at 300 K shown as a function of the first principal axis (PC1) and the second principal axis (PC2). The interval between the contour lines were set to 0.5 kcal/mol for 0−10 kcal/mol (black-blue-purple-red), 1 kcal/mol for 10−20 (red-yellow), 10 kcal/mol for 20−50 (yellow-light pink) and 50 kcal/mol for 50−300 kcal/mol (light pink-light cyan-white). LM1, 2, 3, 4, 5, 6 and LM7 (Aβ 40PCA) are structures of high probability indicative of the associated local minima basins. LM1 is the global minimum structure. Orange horizontal lines define the interface between membrane and solvent, and green horizontal lines define the interface between the lipid headgroup region and the hydrophobic core region of the membrane. The secondary structure is shown by color as red (α-helices), pink (3/10-helices), green (turn), cyan (bend), and white (coil). The side chains of three residues Glu$_{22}$, Asp$_{23}$, and Lys$_{28}$, are shown explicitly. The illustrations were prepared using VMD[85] and Raster3D[86] (b) Free energy landscape of $A\beta_{1-40}$ at 300 K shown at the θ and α axes. The interval between the contour lines are same as (a). The labels LM1, 2, 3, 4, 5, 6, and -LM7 (Aβ40θα) indicate local minima basins. LM1 is the global minimum basin. (c) The local minimum basin structures derived from the PCA are projected onto the θ−α space. The local minima basin structures derived from the PCA (Aβ 40PCA) indicated by dots are LM1 (red), 2 (green), 3 (blue), 4 (magenta), 5 (cyan), 6 (yellow), and LM7 (black).

is located at $(\phi, \psi) = (-60°, -36°)$ and $(\phi, \psi) = (-84°, -6°)$, respectively (see Figure 4, parts (b) and (c)). The global minimum basin structures are populated near the free energy surface minimum (GM) on the $\phi-\psi$ free energy landscape (see Figure 4, parts (d) and (e)). On the basis of our simulations, the structure of residues 23−26 is best represented as a type I β-turn.

Table 1 provides a comparison between peptide secondary structural regions identified from solution phase NMR studies
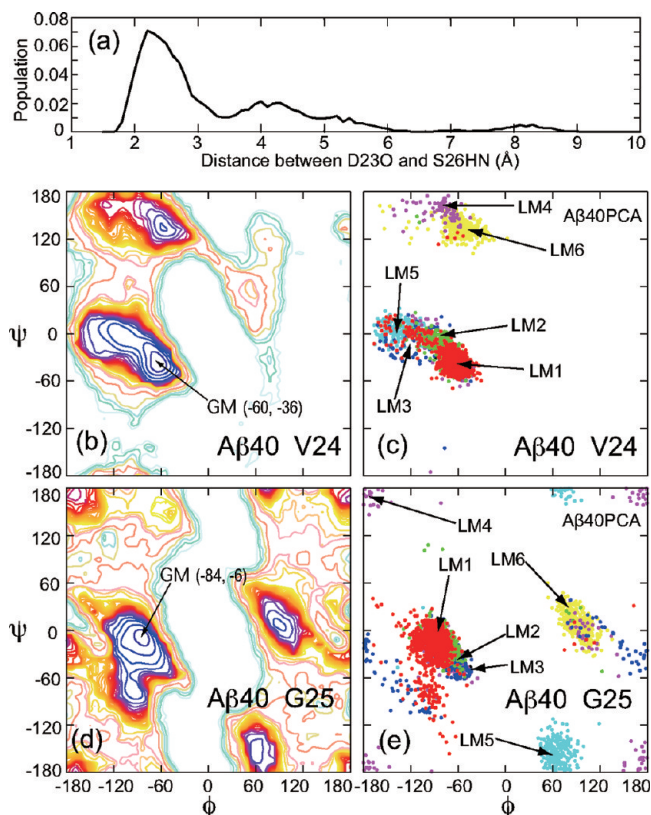
Figure 4. (a) The population of the distance between Asp_{23} O and Ser_{26} HN. The most populated distance is 2.2 Å. The free energy landscapes of $A\beta_{1-40}$ at 300 K projected on the backbone ϕ and ψ axes of residues Val_{24} and Gly_{25} are shown in parts (b) and (d), respectively. GM is global minimum basin. The structures of the PCA (Aβ40PCA) represent LM1(red), LM2(green), LM3(blue), LM4(magenta), LM5(cyan), LM6(yellow), and LM7(black) are projected onto the $\phi-\psi$ space of Val_{24} (c) and Gly_{25} (e).

and our simulations results. The position of the helical regions and intervening turn determined from our simulations are largely consistent with the NMR-derived peptide structures, providing validation for the simulation model and conformational sampling method employed in this study.

The Structure of Aβ_{1-55} in the Membrane Environment. The APP fragment 672−726 (referred to here as $A\beta_{1-55}$) was simulated using REMD and the protocol used in the simulation of $A\beta_{1-40}$. The secondary structure of $A\beta_{1-55}$ at 300 K is shown in Figure 5(a). Residues 13−18 that form domain A_I and residues 30−53 that are included in domain B (30−36) are found to have helical structures separated by a bend region.

The average distributions of the domains A_I (blue), B_{30-36} (magenta), N_ζ of Lys_{28} (red), N_ζ of Lys_{53} (orange), C-terminus (cyan), and N-terminus (green) at 300 K are shown in Figure 5(b). The N_ζ of Lys_{53} and the C-terminus are located on the opposite side of the membrane from the N-terminal domain, A_I domain, and the N_ζ of Lys_{28} suggesting that $A\beta_{1-55}$ acts as a transmembrane domain through the formation of a membrane spanning helix in residues 30−53.

The PCs of the root-mean-square fluctuations of the backbone of the residues 1−40 in $A\beta_{1-55}$ were also calculated. The contribution of the first five PCs are in order: 24.63%, 12.59%, 7.97%, 7.13%, and 4.87%. The first and second PCs, the first and third PCs, and the second and third PCs contribute 37.22%, 32.6%, and 20.56%, respectively. The first and second PCs could serve as good order parameters for the classification of peptide structures. The first and second PC vectors are shown in Figure
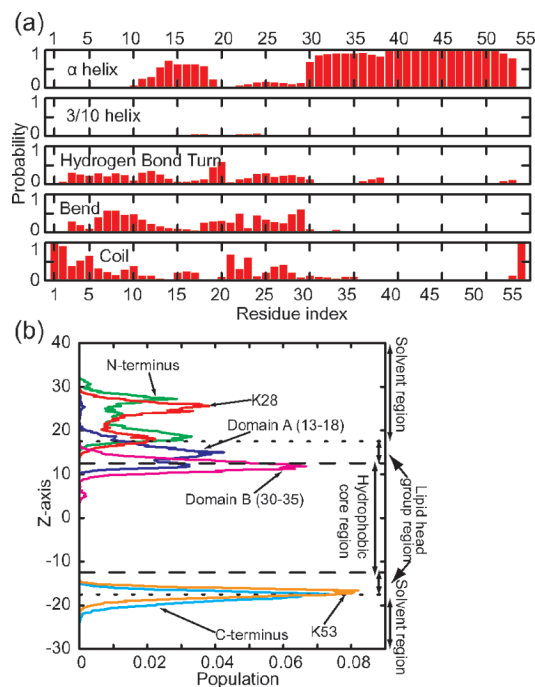
Figure 5. (a) The secondary structure content of residues of $A\beta_{1-55}$ at 300 K. (b) The population of domains and sites of $A\beta_{1-55}$ at 300 K. The dashed and dotted lines indicate the interface between the lipid headgroup region and the hydrophobic core region of the membrane, and the interface between the membrane and solvent. Also shown are the distributions of the position of the N-terminus (green), domain A (13−18) (blue), N_ε at Lys_{28} (red), domain B (30−35) (magenta), C-terminus (cyan), and N_ε of Lys_{53} (orange) projected onto the z-axis, which is normal to the solvent−membrane interface.

6. The first PC is characterized by antiparallel up and down motion of domains A and B along the z-axis, which is normal to the solvent-membrane interface. The second PC is characterized by antiparallel motion to the right and left. Three yellow arrows represent vectors $\vec{a}$, $\vec{b}$, and $\vec{c}$. The definitions of vectors $\vec{a}$ and $\vec{b}$ are identical to those vectors used to analyze $A\beta_{1-40}$. We define domain C (39−52) and vector $\vec{c} = \vec{r}_1 - \vec{r}_2$, where $\vec{r}_1$ and $\vec{r}_2$ are the averaged centers of geometry of the heavy backbone atoms of residues 46−52 and 39−45, respectively. The insertion/tilt angle of domain C (γ) is defined as $\gamma = \arccos(\vec{c} \cdot (-\vec{z}))/(|\vec{c}||\vec{z}|))$.

The free energy landscape projected onto the plane formed by the first and second PC axes at 300 K shows seven local minimum basins (Figure 7 (a)) for $A\beta_{1-55}$ at positions $A\beta$ 55PCA-LM1 (6, −6), LM2 (−26, 6), LM3 (16, −20), LM4 (6, −22), LM5 (−22, −4), LM6 (52, −2), and LM7 (−16, 14). The basins can be classified into four groups. The first group is formed by $A\beta$ 55PCA-LM1 and LM7, the second group contains LM2 and LM5, the third group contains LM3 and LM4, and the fourth group contains LM6. $A\beta$ 55PCA-LM1 is the global minimum basin and has one large transmembrane (TM) helix (30−52) and one short helical domain (13−18). Characteristic structures of the most populated clusters in each basin are shown in Figure 7(a). The free energy difference between the global minimum basin and second local minimum basin is only 0.35 kcal/mol. In spite of this small energetic gap, the global minimum and second local minimum structures present a very different structure in domain A. It is expected that the structure of LM1 would be the dominant structure of $A\beta_{1-55}$ as LM1 has a wide basin as well as the lowest free energy, while basin LM2 is more narrow and would be entropically disfavored.
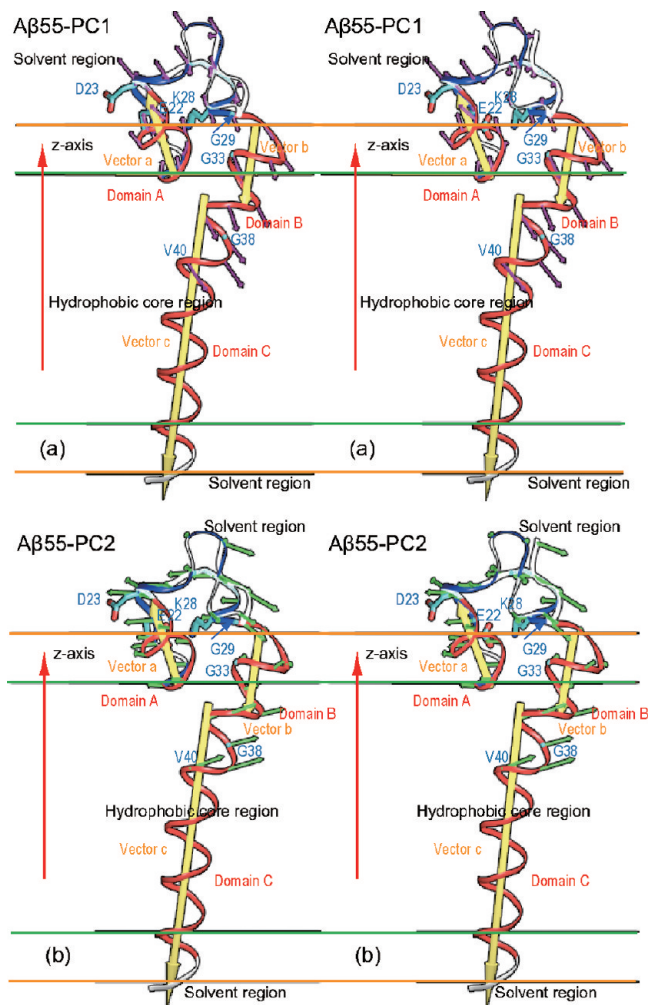
Figure 6. The first (a) and second (b) principal component vectors are depicted in stereo (para) using the global minimum structure of $A\beta_{1-55}$. The vectors (green and orange) extending over residues 1−40 in $A\beta_{1-55}$ portray displacements in the directions of the principal component eigenvectors. See 2 for definitions of graphical elements. This graphic was illustrated using VMD[85] and Raster3D.[86]

The free energy landscape projected onto the interdomain angle (θ) and the tilt angle (α) axes at 300 K is shown in Figure 7(b), with identification of the six local minima. The global minimum basin (LM1) and the second minimum basin (LM2) are located at $(\theta,\alpha) = (99°,21°)$ and $(\theta,\alpha) = (129°,21°)$, respectively. The landscape is characterized by a high wall surrounding a largely flat free energy surface, as the motion of these domains is restricted by the membrane interface and TM domain region. The cluster of structures representing the global minimum $A\beta$ 55PCA-LM1 of the θ-α free energy surface cannot be said to represent the $A\beta_{1-55}$ peptide conformational distribution. A large number of structures are found to be distributed over $A\beta55\theta\alpha$-LM2 and between the $A\beta55\theta\alpha$-LM1 and $A\beta55\theta\alpha$-LM5 (see Figure 7(c)). This result suggests that the tilt angle of the domain B (30−35) fluctuates between the values of $\gamma = 45°$ and 18°. The TM helix spanning residues 30−52 bends about residues Gly37 and Gly38 allowing for fluctuations on the order of 20° in the orientation of domain B relative to the TM helical axis.

The free energy landscape projected onto the α and γ axes is shown in Figure 7(d). The global minimum basin is located at $(\gamma,\alpha) = (24°,21°)$. The orientation of domain B and domain
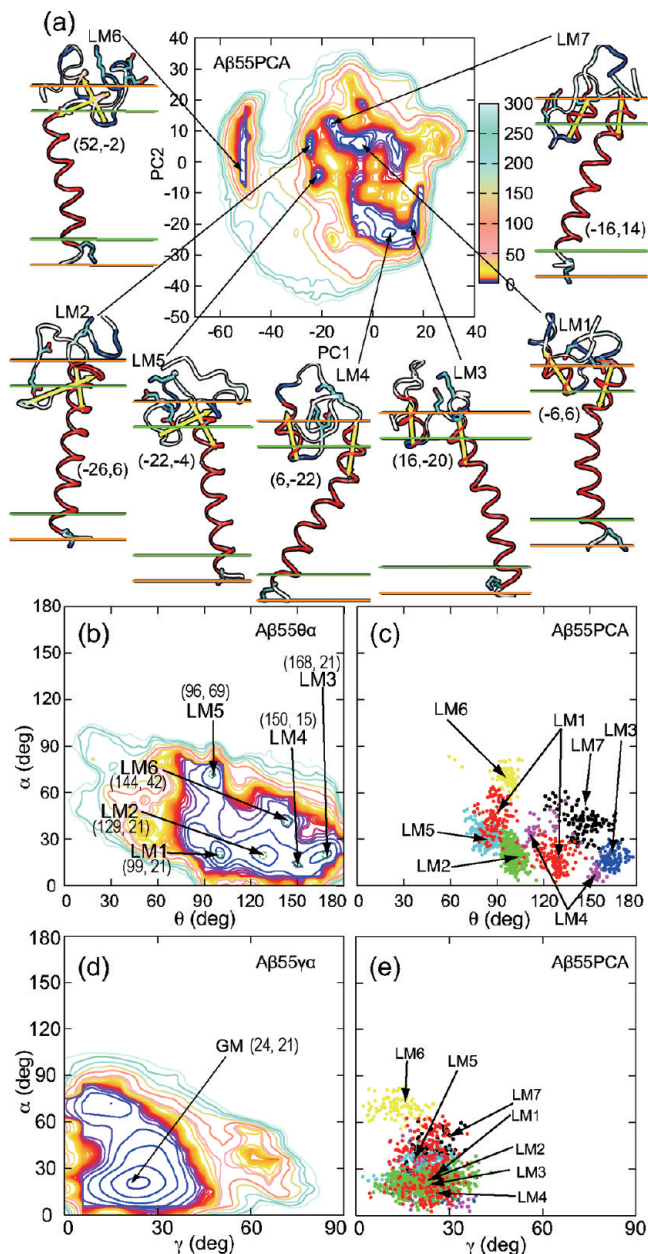
Figure 7. Free energy landscape along the PC1 and PC2 axes at 300 K for $A\beta_{1-55}$. The intervals between the contour lines are set to 0.5 kcal/mol for 0−10 kcal/mol (black-blue-purple-red), 1 kcal/mol for 10−20 (red-yellow), 10 kcal/mol for 20−50 (yellow-light pink) and 50 kcal/mol for 50−300 kcal/mol (light pink-light cyan-white), respectively. Characteristic structures representing the local minima basins are labeled ($A\beta55$PCA)-LM1, 2, 3, 4, 5, 6, and LM7. ($A\beta55$PCA)-LM1 is the global minimum structure. Orange horizontal lines depict the interface between membrane and solvent, and green horizontal lines indicate the interface between the lipid headgroup region and hydrophobic core region in the membrane. The protein's secondary structure is shown by color as red (α-helices), pink (3/10-helices), green (turn), cyan (bend), and white (coil). The six key residues, Glu22, Asp23, Lys28, Glys29, Gly33, and Gly38 are explicitly shown. This graphic was illustrated using VMD[85] and Raster3D[86] (b) Free energy landscape projected on the θ and α axes for the $A\beta_{1-55}$. The interval between the contour lines are same as (a). $A\beta55\theta\alpha$ -LM1, 2, 3, 4, 5, and -LM6 are local minima basins and LM1 is the global minimum basin. (c) The protein structures characteristic of each local minimum basin are projected into the θ−α space. The structures indicated by dots are ($A\beta55$PCA)-LM1(red), 2 (green), 3 (blue), 4 (magenta), 5 (cyan), 6 (yellow), and LM7 (black). (d) Free energy landscape projected on the γ−α plane at 300 K. γ is the angle between the domain C (35−52) vector and the z-axis. The interval between the contour lines are same as (a). (e) The local minimum basin structures characteristic of each local minimum basin were projected onto the γ−α space. The dots are the same as (c).
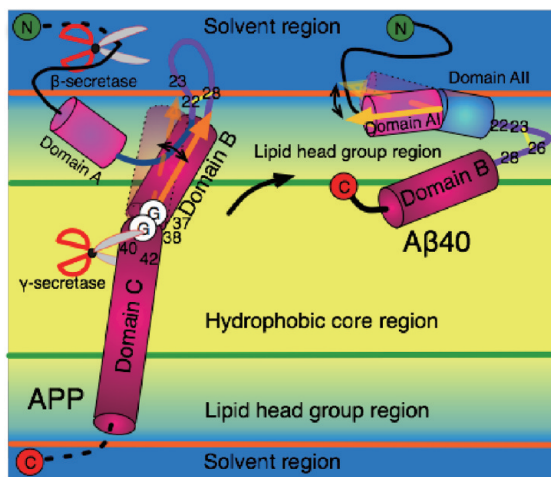
Figure 8. A schematic view of APP ($A\beta_{1-55}$) and $A\beta_{1-40}$ in a membrane. Orange and green lines indicate the interface between the lipid headgroup region and the hydrophobic core region of the membrane, and the interface between the membrane and solvent, respectively. Yellow lines indicate the hydrogen bond (22−28 for APP, 23−26 for $A\beta_{1-40}$). Orange and yellow arrows indicate the vector of domain B in $A\beta_{1-55}$ and the vector of domain A_I in $A\beta_{1-40}$. The helical domains A (13−22), A_I (13−18), A_{II} (19−22), B (30−35), and C (39−52) are represented by cylinders.

C is similar, and sequence 30−55 appears as one straight TM domain. Figure 7(e) shows the projection of each PCA basin structure onto the $\gamma - \alpha$ space. The structures forming the global minimum basin [Aβ55PCA-LM1 (red dots)] are distributed in the region $10° < \alpha < 60°$ and $5° < \gamma < 40°$.

Discussion and Summary

The predicted structures of the $A\beta_{1-40}$ monomer at a membrane interface indicate that the protein structure is characterized by two helical domains A_{13-23} and B_{30-35} separated by a type I β -turn. The secondary structure is similar to that derived from NMR experiment[28] for the $A\beta_{1-40}$ peptide (PDB ID:1AML) in a TFE/water environment (see Table 1). The tertiary structure of the simulated protein differs from the experimentally derived structure in the relative orientation of the helices. The TFE/water environment lacks the interface between the membrane and solvent, which imposes constraints on the relative orientation of the A and B domains of the protein. $A\beta_{1-40}$ is observed to be localized on the interface between the membrane and solvent, which is consistent with the results of long time MD simulations.[42] Domain A is localized atop the hydrophobic core region near the solvent−membrane interface while domain B is found inserted into the hydrophobic core region of the membrane.

The flexibility of the domain A_I (13−18) vector results from the β-turn hinge with significant contributions from the molten nature of the domain A_{II} helix and position of Gly_{29} (see Figure 8). The tilt angle α of $A\beta_{1-40}$ and interdomain angle θ are roughly 45° and 63° in the global minimum structure, repectively. The angles of these domains fluctuate with the constraints imposed by the membrane solvent interface. The flexibility of domain A_I may lead to fluctuations of the peptide associated with its ejection from the membrane.

The structure of $A\beta_{1-55}$ in the membrane has one long TM helix (30−52) that consists of domains B and C, and one small helical domain A (13−18). The secondary structure observed in our simulations of $A\beta_{1-55}$ is similar to that of APP-C99 in the LMPG micelle, proposed based on NMR spectroscopy.[61]

The position of the small helix, which we observed to involve residues 18−22, is somewhat different than has been observed in prior experiment.[61] It is reasonable to assume that the observed difference in the position of the small helix may result from differences between the experimental micelle and simulated membrane environments. The TM helix is observed to bend around Gly_{37} and Gly_{38}, and domain B (30−35) displays significant fluctuations. The peptide residues between Leu_{34} and Leu_{52} are found in the hydrophobic core region of the membrane (see Figure 9).

These results provide insights into the process of creation of $A\beta_{1-40}$ from enzymatic cleavage of APP/APP-C99 (see Figure 8). Lys and Gly residues play important roles in determining the nature of the peptide membrane interaction. Both residues can be located at the interface. We found Lys_{28}, Gly_{29}, Gly_{37}, and Gly_{38} of $A\beta_{1-40}$ to be localized at the interface between the hydrophobic core region and lipid headgroup region in the membrane. Lys_{28}, Gly_{29}, Gly_{33}, Lys_{53}, Lys_{54}, and Lys_{55} of $A\beta_{1-55}$ are located near the interface between the membrane and the solvent. As a result, the Lys residues tend to serve as anchors located at the opposing interfaces. Lys_{28} is located on the upper side of the membrane, while Lys_{54} and Lys_{55} are located on the lower side of the membrane.

The Gly residues can serve as hinges separating the hydrophobic and hydrophilic domains of the peptide. Gly_{38} in $A\beta_{1-55}$ appears to play an important role in stabilizing the TM domain (30−55) region relative to fluctuations in the membrane thickness. The TM domain (30−55) is somewhat longer than our simulated membrane thickness. As a result, the TM domain is observed to bend at Gly_{38}. Through this mechanism, the length of the TM domain can be adjusted to the membrane thickness by the bending or the tilting of the TM domain about the Gly_{38} residue. The tilt angle of domain C is observed to be $\gamma \sim 24°$ and the averaged tilt angle of domain B is $\alpha \sim 21°$. The interdomain angle between domain B and domain C is roughly 177°. Importantly, γ-secretase can bind to the structurally stable domain C neighboring the residue 38−43. In the γ-secretase membrane protein complex, the active site is located in the membrane region. Although the membrane structure will fluctuate, the structure of APP near the γ-site must allow for interaction with the active site of γ-secretase. It is possible that the γ-site, through the incorporation of Gly38, acts as a hinge between domains B and C.

Recently, experimental evidence that APP may exist as a homodimer has been reported.[82,83] In previous work,[84] we predicted the structure of an APP fragment dimer. The hydrophobic core region of the APP fragment was observed to be unchanged in the homodimer conformation. However, the position of Val_{40} in the monomer peptide was observed to be closer to the membrane interface. The tilt angle of $A\beta_{1-55}$ observed in this study is 2× larger than the average tilt angle of the previous study.[84] In the absence of a better understanding of the structure of the γ-secretase complex, it is unclear how those structural perturbations may affect cleavage. However, we have demonstrated that Gly_{38} in the dimer acts as a hinge between the Gly-xxx-Gly interface and domain C. We conjecture that Gly_{38} plays a crucial role in allowing domains B and C to

(84) Miyashita, N.; Straub, J. E.; Thirumalai, D.; Sugita, Y. *J. Am. Chem. Soc.* **2009**, *131*, 3438–3439.
(85) Humphrey, W.; Dalke, A.; Schulten, K. *J. Mol. Graphics* **1996**, *14*, 33–38.
(86) Merritt, E.; Murphy, M. *Acta Cryst. D, Biol. Cryst.* **1994**, *50*, 869–873.
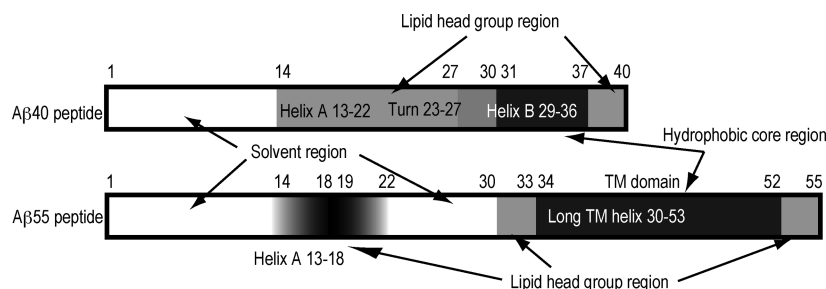
Figure 9. The membrane regions of $A\beta_{1-40}$ and $A\beta_{1-55}$ are shown, where white, gray, and black indicate the solvent region, the lipid headgroup region, and the hydrophobic core region, respectively. Light gray or dark gray (gradation) are used if the residues are close to the solvent or hydrophobic core regions.

maintain a position near the γ-site in the membrane. It will be prudent to evaluate how the flexibility of those APP domains, influenced by the composition of the APP sequence, is correlated with γ-secretase activity.

The TM domain includes the domain B (30−35) in $A\beta_{1-55}$. However, following APP-C99 cleavage by γ-secretase, domain B aligns with the membrane surface. The domains in the solvent region, especially 22−29, are pulled into the membrane region leaving the C-terminal region of $A\beta_{1-40}$ located in the membrane region. The VGSN (24−27) region and the salt bridge between Asp_{23} and Lys_{28} have been identified as key structural elements of the monomer and fibril structures of $A\beta$ peptide in solution.[13,15,17,37−41] In our simulations of the membrane $A\beta_{1-40}$ peptide system, Asp_{23} does not contact Lys_{28}, while Asp_{23} O and Asn_{27} N are observed to form a stabilizing contact. The peptide is observed to from a type I β-turn, but the side chains do not face each other. The side chains of Glu_{22} and Asp_{23} are located in the solvent regions, and Lys_{28} is located in the lipid headgroup region.

In predicted structures of the APP ($A\beta_{1-55}$ peptide), the VGSN region is localized in the solvent region and consists of a loop. Glu_{22} and Lys_{28} are located on the interface between the solvent region and the lipid headgroup region, and a salt bridge is formed between these side chains. The VGSN and neighboring residues are typically observed to form bend, turn or loop structures. It is clear that the hydrogen bonding structure would be changed through the process APP/APP-C99 → $A\beta$ peptide in membrane → soluble $A\beta$ peptide → oligomer/fibril structure. The pillowy region 19−22, namely domain A_{II} in $A\beta_{1-40}$, is also deformed during the release of $A\beta_{1-40}$ from APP. Domain B tends to maintain a helical structure that is perpendicular to the membrane surface (with a tilt angle of 99°). The N-terminal side of domain B (around Ala_{30}) of $A\beta_{1-55}$ is located on the outside of the membrane, while the Ala_{30} of $A\beta_{1-40}$ is located in the lipid headgroup region, close to the hydrophobic core region. We observe that domain A_I of both $A\beta_{1-40}$ and $A\beta_{1-55}$ is predominantly found oriented along the membrane interface.

The domain A_{II} region of $A\beta_{1-55}$ tends to be observed outside the membrane near domain B, while domain A_{II} of $A\beta_{1-40}$ tends to be observed within the membrane region. The domain A_{II} region is observed to be helical in the membrane environment and a coil in an aqueous environment. The A_{II} region is extended in APP due to tension centered in the 20−28 loop region, but A_{II} forms a helix in $A\beta_{1-40}$ by the relaxation of this tension following peptide cleavage.

Considerable attention has been given to the consequences of the two residues defining the difference between $A\beta_{1-40}$ and $A\beta_{1-42}$. It has been speculated that the addition of two
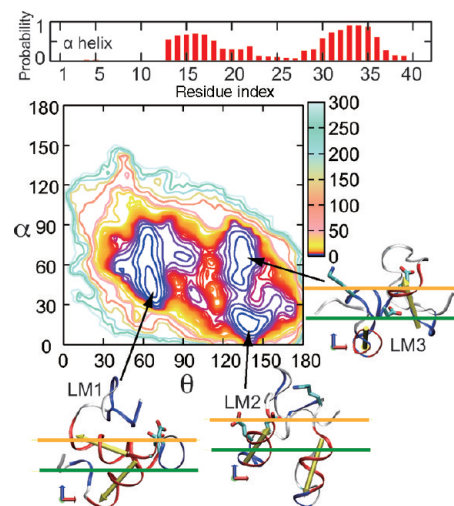
Figure 10. The α helix content for residues of $A\beta_{1-42}$ and free energy landscape along the θ and α axes for $A\beta_{1-42}$ at 300 K. The interval between the contour lines is set to 0.5 kcal/mol for 0−10 kcal/mol (black-blue-purple-red), 1 for 10−20 (red-yellow), 10 for 20−50 (yellow-lightpink) and 50 for 50−300 kcal/mol (lightpink-light cyan-white). The labels LM1, 2, and LM3 indicate local minima basins. LM1 is the global minimum basin.

hydrophobic residues to the C-terminal region of the peptide may be responsible for the enhanced aggregation propensity observed in some experimental studies. Following the protocol described for the simulation of $A\beta_{1-40}$ in this study, we have also simulated the conformational ensemble of $A\beta_{1-42}$ in the implicit membrane environment. We show the free energy surface along the θ and α axes in Figure 10. Basin LM1 is separated from LM2 by a high free energy barrier (10 kcal/mol) at $A\beta_{1-42}$. The free energy surface is somewhat different between $A\beta_{1-40}$ and $A\beta_{1-42}$. The most probable structures for $A\beta_{1-40}$ and $A\beta_{1-42}$ are displayed in Figure 3(a) LM1 and 10 LM1. In spite of the presence of two additional hydrophobic residues in the C-terminal region of $A\beta_{1-42}$, no significant difference in the most probable structures of $A\beta_{1-40}$ and $A\beta_{1-42}$ is observed in our simulations. This is somewhat different from the conclusion of the earlier study by Mobley et. al[58] that noted differences in the degree of insertion of $A\beta_{1-40}$ and $A\beta_{1-42}$. We note that our study uses a slightly different computational model, but also has a more complete sampling of the peptide conformational ensemble than was feasible in that earlier work.

In summary, we have studied the structure of the $A\beta_{1-40}$, $A\beta_{1-42}$, and APP/APP-C99 fragment ($A\beta_{1-55}$) in a membrane environment using replica exchange molecular dynamics simulation and free energy analysis. The structures and conformational change during the release of $A\beta_{1-40}$ peptide from APP

are largely affected by the system environment, including the solvent regions, lipid headgroup regions, and hydrophobic core region. The C-terminal sequence of both peptides favors the membrane region, and the 13 residue N-terminal sequence favors the solvent region and forms a coil. $A\beta_{1-40}$ favors the lipid headgroup region and solvent region, and the APP fragment ($A\beta_{1-55}$) has a long TM domain (30−55) in the opposing lipid headgroup regions and hydrophobic core region. Residue 30−55 in the APP fragment forms a transmembrane helix. The disappearance of the helix following cleavage at the γ-secretase cleavage site enhances the structural change. The structures of domain A_{II} and the loop/turn regions are modified by the system environment.

The results of our study provide a structural basis for the docking of APP with γ-secretase, an essential step in the creation of $A\beta$ peptide from APP. In particular, the intrinsic flexibility observed in the simulated transmembrane sequence of APP, modeled as $A\beta_{1-55}$, in the vicinity of the γ-site may be essential in facilitating interaction between the APP protein and the active site of γ-secretase (see Figure 8). Depending on the peptide sequence and local structure, the splicing position can vary, resulting in $A\beta$ peptide fragments of different length. The results of this study suggest that sequence variations in APP, some of which are associated with the early onset of amyloid disease, may effect the population and distribution of $A\beta$ peptide isoforms in a way that influences the overall process of amyloidosis.

In closing, we note that APP is known to form homodimers in a membrane environment, structures stabilized by interpeptide contacts encoded by the Gly-xxx-Gly sequence motif. Recently, we carried out a simulation study of a transmembrane APP fragment ($A\beta_{23-55}$) homodimer in a membrane environment.[84] That study led to putative homodimer structures for both the wild-type protein and a mutant. Our combined studies lead to important conjectures regarding how sequence may inform the angle of peptide insertion in a membrane and subsequent peptide cleavage, considerations that are essential aspects of $A\beta$ peptide production in the initial stages of the aggregation pathway.